Analysis of $\psi\prime(J/\psi) \to K1^{\pm}(1270)K^{\mp}; K1^{\pm}(1400)K^{\mp}$

Ban Yong
Technical Physics Department, Peking University
(Email: 'bany@bepc5.ihep.ac.cn", or, 'yban@hs651.bimp.pku.edu.cn")

June 18, 1998, BES Annual Meeting, Datong

Abstract

Using the $\psi\prime$ data collected by the BES detector from 1993 to 1995, the decays $\psi\prime(J/\psi) \to K_1^{\pm}(1270)K^{\mp}$ and $\psi\prime(J/\psi) \to K_1^{\pm}(1400)K^{\mp}$ are analyzed. The preliminary branching ratios are calculated, and their physics implication are explored . The results are in consistent with the Hawaii group's analysis for the same decays.

1 Motivation

In this work we have analyzed the hadronic decays $\psi\prime(J/\psi) \to K_1^{\pm}(1270)K^{\mp}$ and $\psi\prime(J/\psi) \to K_1^{\pm}(1400)K^{\mp}$ using BES $\psi\prime$ data. The subject was proposed by the Hawaii group, and they got some interesting results which can not be explained by the current theory [1]. An independent analysis using the same data set was needed.

- The "15% rule" gives that [2], the ratio between the $\psi\prime$ and J/ψ decay to the same hadronic channel is near 15%. Most of the hadronic channels satisfy this rule; however, some large discrepancy were found in some VP channels [3], and recently in some VT channels (by BES experiment). No satisfactory explanation was accepted by now. It is important to testify the "15% rule" in other decay modes, such as the AP mode in the current analysis.

- The observed $K_1(1270)$ and $K_1(1400)$ particles are the mixtures of the two strange members (K_A and K_B) of the two $^3P_1$ and $^1P_1$ octets with the mixing angle θ near 45^o [4]:

$$K_1(1270) = sin\theta K_A + cos\theta K_B \qquad (1)$$

$$K_1(1400) = cos\theta K_A - sin\theta K_B \qquad (2)$$

Or,

$$K_A = sin\theta K_1(1270) + cos\theta K_1(1400) \qquad (3)$$

$$K_B = cos\theta K_1(1270) - sin\theta K_1(1400) \qquad (4)$$

In the flavor-SU(3) symmetry, the amplitude for two body decays to conjugate mesons in the same pair of octets are equal. In case of $\psi\prime$ and J/ψ decays, the amplitude of the decay $\psi\prime(J/\psi) \to K_A\bar{K}$ should equal to that of $\psi\prime(J/\psi) \to a_1\pi$, while the later decay is forbidden by G-parity conservation. Thus one expects relatively pure $K_B\bar{K}$ final states in the observed $\psi\prime(J/\psi) \to K_1 K$ decays. From the above equation one would expect equal amounts of $K_1(1270)$ and $K_1(1400)$ since the mixing angle θ is nearly 45^o. Thus, by measuring their branching ratios, the flavor-SU(3) symmetry can be tested.

2 Selection Procedure

- final state particles: The dominant decay modes of $K_1(1270)$ are to $K\rho$ (42%), $K_0^*(1430)\pi$ (28%) and $K^*(892)\pi$. Most of $K_1(1400)$ decays to $K^*(892)\pi$ (94%), while a small part decays to $K\rho$ (3%). We choose the most prominent decay modes in both decays which will lead to the same final state particles $K^+K^-\pi^+\pi^-$. Considering the isospin decomposition in each step, the following branching fraction are obtained for those channels:

$$
\begin{array}{llll}
\psi\prime(J/\psi) \to K_1^{\pm}(1270)K^{\mp} & \to (K\rho)^{\pm}K^{\mp} & \to K^+K^-\pi^+\pi^- & = 0.14 \pm 0.02 \\
 & \to (K^*\pi)^{\pm}K^{\mp} & \to K^+K^-\pi^+\pi^- & = 0.07 \pm 0.02 \\
\psi\prime(J/\psi) \to K_1^{\pm}(1400)K^{\mp} & \to (K^*\pi)^{\pm}K^{\mp} & \to K^+K^-\pi^+\pi^- & = 0.42 \pm 0.03 \\
 & (\to (K\rho)^{\pm}K^{\mp} & \to K^+K^-\pi^+\pi^- & = 0.01 \pm 0.01)
\end{array}
$$

- Data Sample: The $e^+e^- \to \psi\prime$ data (center of mass energy 3.686 GeV) collected by BES detector was used. The total number of $\psi\prime$ events is $(3.788 \pm 0.009 \pm 0.310) \times 10^6$. It was collected during two periods: December 1993 to January 1994 (totally $(1.325 \pm 0.005 \pm 0.108) \times 10^6$ $\psi\prime$ events), and January to April 1995 (totally $(2.463 \pm 0.007 \pm 0.202) \times 10^6$ $\psi\prime$ events). The J/ψ data used in our analysis was extracted from the same data sample, using the decay $\psi\prime \to \pi^+\pi^- J/\psi$.

  The $\psi\prime$ data was stored in several groups according to the number of charged prongs presented in the event. We use 4-prong and 6-prong data for $\psi\prime$ and J/ψ analysis respectively. We discarded the runs with QRUN (flag indicating the quality of the data) equals to 0 ("bad run"), and kept the runs with QRUN=3 (good quality, account for 86% of the total data), or QRUN=1,2 (having some problems but usable). For different run quality data, we have checked the ratio between the number of selected events and the total number of events, and found these ratio are consistent for data with different run quality.

- Monte Carlo Simulation: The HOWL generator was used which will generate events according to the phase space distribution. Totally six different samples of Monte Carlo are generated, with 2000 events for each sample (the channel $K_1(1400) \to K\rho^0$ is very small (3%), thus can be neglected and the process was not generated):

  - $\psi\prime \to K_1^{\pm}(1270)K^{\mp}; K_1^{\pm}(1270) \to K^{\pm}\rho^0(770); \rho^0(770) \to \pi^+\pi^-$:
  - $\psi\prime \to K_1^{\pm}(1270)K^{\mp}; K_1^{\pm}(1270) \to K^{*0}(892)\pi^{\pm}; K^{*0}(892) \to K^{\pm}\pi^{\mp}$;
  - $\psi\prime \to K_1^{\pm}(1400)K^{\mp}; K_1^{\pm}(1400) \to K^{*0}(892)\pi^{\pm}; K^{*0}(892) \to K^{\pm}\pi^{\mp}$;

- $\psi\prime \rightarrow \pi^+\pi^- J/\psi; J/\psi \rightarrow K_1^{\pm}(1270)K^{\mp}; K_1^{\pm}(1270) \rightarrow K^{\pm}\rho^0(770); \rho^0(770) \rightarrow \pi^+\pi^-$
- $\psi\prime \rightarrow \pi^+\pi^- J/\psi; J/\psi \rightarrow K_1^{\pm}(1270)K^{\mp}; K_1^{\pm}(1270) \rightarrow K^{*0}(892)\pi^{\pm}; K^{*0}(892) \rightarrow K^{\pm}\pi^{\mp}$;
- $\psi\prime \rightarrow \pi^+\pi^- J/\psi; J/\psi \rightarrow K_1^{\pm}(1400)K^{\mp}; K_1^{\pm}(1400) \rightarrow K^{*0}(892)\pi^{\pm}; K^{*0}(892) \rightarrow K^{\pm}\pi^{\mp}$;
- for each sample we generated equal number of events for two different charge conjugate processes.
- The detector condition are somewhat different in 1993-1994 and 1995 periods, the events in each samples are generated for these two conditions separately, their numbers are determined according to the relative luminosity corresponding to the two periods.

3 Selection of Event

The procedure of event selection is illustrated by the flow diagram in the next page. Since the same data sample was used to analyze both $\psi\prime$ and J/ψ decays, the same criteria in the event selections in both analysis are applied, in order to reduce the systematic effect when comparing the branching ratios of the two.

- Pre-selection

  Data samples with $K^+K^-\pi^+\pi^-$ tracks which could be resulted from $K_1^{\pm}K^{\mp}$ are selected. For 6-prong data, another pair of $\pi^+\pi^-$ recoiling to J/ψ should also be identified. Some conventional selection cuts used in BES analysis are applied here.

  - Track selection: for 4-prong data, we require the event has 4 charged tracks; each track has the charge equals to +1 or -1; MFIT equals to 2; and $cos\theta \leq 0.8$ (where MFIT is the parameter indicating the track fitting quality, θ is the polar angle of the track). The sum of the charge of the 4 tracks should be zero. For 6-prong data the same requirements were applied to each track. About 20% of 4-prong events and 8% of 6-prong events passed these cuts.
  - Apply corrections to the reconstructed parameters: three subroutines developed by $\psi\prime$ group are called: "vxkwik" will give a vertex correction, and the position of the shower counter first layer hits are corrected accordingly. The events with no vertex found are discarded. The vertex of the selected events has z position within 15 cm to the interaction point, and the distance to the beam axis less than 2 cm. The subroutine "dedxpsip" "tofpsip" will recalculate the particle identification $\chi^2(dE/dx)$ values (number of σ from hypothesis) and the particle identification TOF weight values for $\psi\prime$ data respectively. The corrected values are used in the analysis.
  - For 6-prong data, select the event which has a $(\pi^+\pi^-)$ pair recoiling to J/ψ (the candidates of $\psi\prime \rightarrow \pi^+\pi^-(J/\psi)$ and $J/\psi \rightarrow K^+K^-\pi^+\pi^-$). The searching can be performed by calculating the recoil mass of any combination of the opposite charged track pairs using the measured track momentum; or by a kinematic fit with a resonance at J/ψ mass, looping over all of the opposite charged track pair assumptions. We tried

the both method and found they give exactly the same pair of tracks. Fig.1 gives the recoil mass distributions of the two $\pi^+\pi^-$ pairs, a clear peak in the J/ψ mass region is presented.

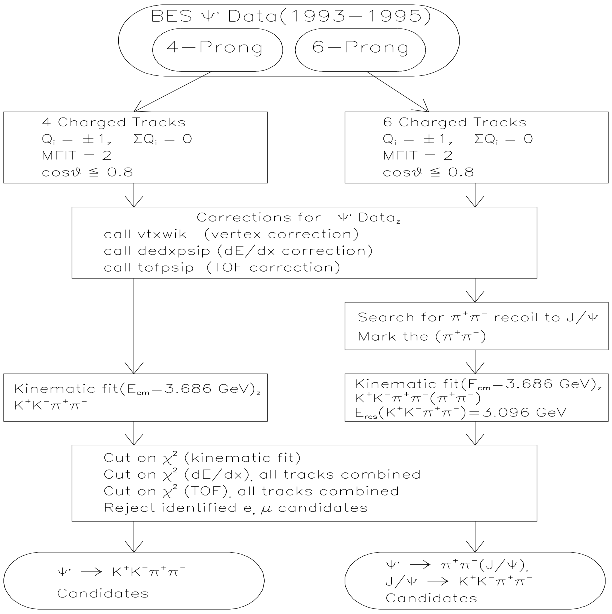

The flow diagram in event selection.

The events with the recoil mass of a $\pi^+\pi^-$ pair in the J/ψ mass region ($M(\pi^+\pi^-) \subset$ [3.05, 3.15] GeV/c^2) are selected for the $\psi\prime \to \pi^+\pi^- J/\psi, J/\psi \to K^+K^-\pi^+\pi^-$ analysis.

– The kinematic fit using "telesis" package then applied. For the 4-prong data, the fits are looped over all combinations of $K^+K^-\pi^+\pi^-$ track assumptions. We included the dE/dx information in the fit: the χ^2 of the fit is combined with the χ^2 of the track identification with dE/dx information. The total χ^2 is defined as:

$$\chi^2 = \chi^2(fit) + \sum_{i=1}^{4} \chi^2(dE/dx) \tag{5}$$

Including the $\chi^2(dE/dx)$ term in the fit will significantly improve the mass resolution and increase the efficiency. $\sum \chi^2(TOF)$ can also be included, but we found this term doesn't have much effect on the result. The total degree of freedom becomes 8 after including the $\chi^2(dE/dx)$ term. For 6-prong data, the $\pi^+\pi^-$ pair recoiling to J/ψ are identified in the above procedure, the remaining four tracks are looped over for all combinations of $K^+K^-\pi^+\pi^-$ track assumptions. We also included the $\sum \chi^2(dE/dx)$ (for all 6 tracks) in the total χ^2 of the fit. Taking into account the resonance mass constraint for $J/\psi \to K^+K^-\pi^+\pi^-$, the total degree of freedom becomes 11. Fig.2 shows the mass distributions of $\pi^+\pi^-$, the χ^2 and probability of the fit with or without the term $\sum \chi^2(dE/dx)$ (for $\psi\prime \to K_1^{\pm}(1270)$ Monte Carlo). It is clear that the efficiency is increased and the mass resolution is improved. Finally a cut at the combined probability of the fit ($prob(\chi^2(fit) + \sum \chi^2(dE/dx), n) > 0.03, n$ is the degree of the freedom) is applied.

- More cuts on track identification parameters based on dE/dx and TOF information are applied: if the probability $prob(\chi^2, 1)$ of any track for K or π assumptions after the fit is less than 0.001, the track is discarded. The χ^2 of the remained tracks are summed over, and a cut at the combined probability ($prob(\sum \chi^2, n) > 0.03$) is applied for dE/dx and TOF informations respectively. We concluded that the particle identification assigned by the kinematic fit are consistent with dE/dx and TOF identification.
- Cuts to remove electron and muon track candidates are also applied: the track is regarded as an electron if: for track with $P > 1$ GeV/c, the ratio E_{SC}/P is greater than 1; or for any pair of + - charged tracks both having $P > 1$ GeV/c, the quantity $[(E_{SC}/P)_+ - 1]^2 + [(E_{SC}/P)_- - 1]^2$ is less than 0.36. The tracks are regarded as the muon candidates if: the sum of the numbers of the muon counter layer hits for any pair of positive and negative charged tracks is equal to or greater than 3. Actually these cuts have no effect on the 6-prong events selected by the previous procedure, but they removed some contamination in the selected 4-prong events come from $\psi\prime \to \pi^+\pi^- J/\psi$ and $J/\psi \to$ two charged tracks which are mis-identified as K^+K^- pairs. Those events can also be removed by a cut at the invariant mass of K^+K^- candidates in the J/ψ mass region, see below.

- Further Cuts

  The selected 6-prong events passing the above criteria are the quite clean sample of $\psi\prime \to \pi^+\pi^-(J/\psi)$ and $J/\psi \to K^+K^-\pi^+\pi^-$, while most of the selected 4-prong events come from the contamination of $\psi\prime \to \pi^+\pi^- J/\psi$, and $J/\psi \to$ two charged tracks which are mis-identified as K^+K^- pairs.

  - Remove $\psi\prime \to \pi^+\pi^- J/\psi$ in the selected 4-prong data sample. A clear high peak centered at J/ψ mass was seen in the distribution of the invariant mass of the K^+K^- track candidates. This peak was excluded by a cut at $M(K^+K^-) < 3.05$ GeV/c^2 or $M(K^+K^-) > 3.15$ GeV/c^2. Nearly 90% of events are removed by this cut. Fig.3 shows the distributions of the invariant mass of the $\pi^+\pi^-$ track candidates and the K^+K^- track candidates. After this cut, the $\rho(770)$ peak is clearly seen in the $\pi^+\pi^-$ mass distribution. On the other hand, no signal of the J/ψ peak was seen in the invariant mass distributions of the K^+K^- track candidates in the selected 6-prong events sample.
  - A peak near the low end of K^+K^- mass distributions comes from the event of $\psi\prime(J/\psi) \to \phi(1020)X$, and $\phi(1020) \to K^+K^-$ (the branching fraction is 49.2%), $X \to \pi^+\pi^-$. These events are removed by a cut at $M(K^+K^-) > 1.04$ (GeV/c^2). Fig.4 gives the invariant mass distributions of $\pi^+\pi^-$ and K^+K^- for 4-prong data, the $\phi(1020)$ peak is also shown. The invariant mass peak of $\pi^+\pi^-$ near 1 (GeV/c^2) recoil to $\phi(1020)$ is likely come from $f_0(980)$ which decay to $\pi\pi$ with a branching fraction of 78.1%. The similar $\phi(1020)$ peak can also be seen in the 6-prong data, while the peak near 1 (GeV/c^2) in $\pi^+\pi^-$ mass distribution is not so obvious.
  - The helicity angle cut: for $K_1^\pm(1270)K^\mp$ analysis ($K_1^\pm(1270) \to K^\pm\rho^0(770) \to K^\pm\pi^+\pi^-$), the helicity angle θ is defined as the angle between the $\rho^0(770)$ and the

$K^{\mp}$ recoiling to $K_1^{\pm}(1270)$ in the $K_1^{\pm}(1270)$ rest frame; for $K_1^{\pm}(1400)K^{\mp}$ analysis ($K_1^{\pm}(1400) \rightarrow K^{*0}(892)\pi^{\pm} \rightarrow K^{\pm}\pi^{+}\pi^{-}$), θ is defined as the angle between the $K^{*0}(892)$ and the $K^{\mp}$ recoiling to $K_1^{\pm}(1400)$ in the $K_1^{\pm}(1400)$ rest frame. A peak near 1 is presented in $cos\theta$ distribution for $\psi\prime(J/\psi) \rightarrow K_1(1270)K$ Monte Carlo, while no obvious peak was seen in $cos\theta$ distribution for $\psi\prime(J/\psi) \rightarrow K_1(1400)K$ Monte Carlo. We applied a cut at $cos\theta < 0.75$ in $\psi\prime(J/\psi) \rightarrow K_1(1270)K$ analysis. This cut effectively removed the wrong combinations of $K^{\pm}\pi^{+}\pi^{-}$ which is not from the K_1 decay.

- Event Numbers After Each Selection Step

Table 1 gives the event numbers in different selection steps after various cuts described above, except for the helicity angle cut. The number of events of different run quality data, the number of event without neutral track and the number of the events which has more than one barrel shower counter hits are also listed. After the relatively loose cuts ($CL.(fit+dE/dx)$; $CL.(\Sigma dE/dx)$ and $CL.(\Sigma TOF) \geq 0.01$) all event and track information are filled in Ntuple for further studies.

Table 1. Statistics In Event Selection

Sample	4-prong Data	6-prong Data
Total Events	2323694	1749417
(Run Quality=1	86128	57198)
(Run Quality=2	230143	178122)
(Run Quality=3	1943270	1481879)
Good Run	2259541	1717199
Cuts on tracks (MFIT=2,cosθ <0.8 etc.)	435273	140577
(without neutral track	36535	3272)
(at least 1 BSC hit	395146	136325)
Kinematic fit ($CL.(fit + dE/dx) \geq 0.01$	8974	658
$CL.(\Sigma dE/dx) \geq 0.01$	8666	640
$CL.(\Sigma TOF) \geq 0.01$	8071	535
More strict cuts ($CL.(fit + dE/dx), CL.(\Sigma dE/dx), CL.(\Sigma TOF) \geq 0.03$)	5575	427
Remove electron candidate	5558	423
Remove muon candidate	4556	423
Remove J/ψ contamination	596	423
Remove $\psi\prime(J/\psi) \rightarrow \phi X$	542	395

- Mass Distribution

The scatter plots of the invariant mass distributions for $\pi^{+}\pi^{-}$ .vs. $K^{\pm}\pi^{+}\pi^{-}$ and $K^{\pm}\pi^{\mp}$ .vs. $K^{\pm}\pi^{+}\pi^{-}$ are displayed respectively for 4-prong data and 6-prong data in Fig.5. Here two possible particle combinations for each events ($K^{+}\pi^{+}\pi^{-}$ or $K^{-}\pi^{+}\pi^{-}$) are filled (2 entries/ per event). The band of $K^{*}(892)$ mass are seen quite clearly in $M(K^{\pm}\pi^{\mp})$ dimension for both 4-prong and 6-prong data, the $\rho(770)$ band are also seen for 4-prong data but not so obvious for 6-prong data. Some clustering of event near $K_1(1270)$ or $K_1(1400)$ mass are seen in $M(K^{\pm}\pi^+\pi^-)$ dimension for the 4-prong data, but not so obvious for the 6-prong data. Further cuts on $M(\pi^+\pi^-)$ and $M(K^{\pm}\pi^{\mp})$ near $\rho(770)$ and $K^*(892)$ mass will give the candidates of the events coming from $\psi\prime(J/\psi) \rightarrow K_1(1270)$ or $\psi\prime(J/\psi) \rightarrow K_1(1400)$ respectively.

Fig.6 gives the invariant mass distributions of $K^{\pm}\pi^+\pi^-$ for 4-prong data and for 6-prong data respectively after the $\rho(770)$ mass cut. The effect of removing $\psi\prime(J/\psi) \rightarrow \phi X$ events and the effect of the helicity angle cut are also shown. Most of the wrong combinations are removed by the $cos\theta < 0.75$ cut. The bottom plots shows the final $M(K^{\pm}\pi^+\pi^-)$ distributions after the cut at $\rho(770)$ mass (require $|M(\pi^+\pi^-) - M(\rho(770))| < 0.15$ GeV/c^2), the $K_1(1270)$ peak is seen in the $M(K^{\pm}\pi^+\pi^-)$ distributions for the 4-prong data ($\psi\prime \rightarrow K_1K$), while there seem to be also a heap around 1.4 GeV/c^2 for the 6-prong data ($J/\psi \rightarrow K_1K$).

Fig.7 gives the invariant mass distributions of $K^{\pm}\pi^+\pi^-$ for 4-prong data and for 6-prong data respectively after the $K^*(892)$ mass cut . The effect of removing $\psi\prime(J/\psi) \rightarrow \phi X$ events are shown by the shadowed area in the top plots (2 entries / per event). Applying a $K^*(892)$ mass cut ($|M(K^{\pm}\pi^{\mp}) - M(K^*(892)| < 0.05$ GeV/c^2), the resulted $K^{\pm}\pi^+\pi^-$ distributions are shown in the bottom plots (also the dark area in the top plots). The $K_1(1400)$ peak is seen in the $M(K^{\pm}\pi^+\pi^-)$ distributions for the 6-prong data ($J/\psi \rightarrow K_1K$), while there seem to be a overlap of $K_1(1400)$ and $K_1(1270)$ in the distribution for the 4-prong data ($\psi\prime \rightarrow K_1K$).

4 Branching Ratios

The events appeared in the peak of $K_1(1270)$ mass region after the ρ mass cut may come from two decays: $K_1(1270) \rightarrow K\rho \rightarrow K\pi\pi$, or $K_1(1270) \rightarrow K^*\pi \rightarrow K\pi\pi$ while the final $M(\pi\pi)$ happenly satisfy the ρ mass cut. Since the branching ratios of the 2 decays are comparable, the later case can not be neglected. Denoting the efficiencies for the two process as $\epsilon_{\rho\ cut}^{K_1(1270)\rightarrow K\rho}$ and $\epsilon_{\rho\ cut}^{K_1(1270)\rightarrow K^*\pi}$, the true $K_1(1270)K$ event number $N_{true}^{K_1(1270)}$ can be derived by applying the correction factors to the observed $K_1(1270)K$ event number $N_{obs.}^{K_1(1270)}$. The branching ratio of $\psi\prime \rightarrow K_1^{\pm}(1270)K^{\mp}$ is:

$$Br(\psi\prime \rightarrow K_1^{\pm}(1270)K^{\mp}) = \frac{N_{true}^{K_1(1270)}}{N_{\psi\prime}} \tag{6}$$

$$= \frac{N_{obs.}^{K_1(1270)}}{N_{\psi\prime}[Br_{K_1(1270)\rightarrow K\rho\rightarrow K\pi\pi} \times \epsilon_{\rho\ cut}^{K_1(1270)\rightarrow K\rho} + Br_{K_1(1270)\rightarrow K^*\pi\rightarrow K\pi\pi} \times \epsilon_{\rho\ cut}^{K_1(1270)\rightarrow K^*\pi}]} \tag{7}$$

The branching ratio of $\psi\prime \rightarrow K_1^{\pm}(1400)$ is measured via a cut at K^* mass. Since the branching ratio of the decay $K_1(1400) \rightarrow K\rho$ is very small compared with the branching ratio of the decay $K_1(1400) \rightarrow K^*\pi$, the $K_1(1400)$ events come from $K_1(1400) \rightarrow K\rho$ with $M(K\pi)$ happenly satisfying the K^* mass cut can be neglected. By similar symbol, the branching ratio of $\psi\prime \rightarrow K_1^{\pm}(1400)K^{\mp}$ is:

$$Br(\psi\prime \rightarrow K_1^{\pm}(1400)K^{\mp}) == \frac{N_{obs.}^{K_1(1400)}}{N_{\psi\prime}Br_{K_1(1400)\rightarrow K^*\pi\rightarrow K\pi\pi} \times \epsilon_{K^*\ cut}^{K_1(1400)\rightarrow K^*\pi}} \tag{8}$$

The branching ratio of $J/\psi \rightarrow K_1 K$ can be calculated by similar equations as above, but $N_{\psi\prime}$ should be replaced by the total J/ψ number $N_{J/\psi}$. Since the J/ψ sample is selected via $\psi\prime \rightarrow \pi^+\pi^-(J/\psi)$ decay, the total J/ψ number $N_{J/\psi} = N_{\psi\prime} \times Br(\psi\prime \rightarrow \pi^+\pi^-(J/\psi))$ while the branching ratio of the decay $\psi\prime \rightarrow \pi^+\pi^-(J/\psi)$ is given in PDG [5].

- Efficiency

  The efficiencies for different processes are calculated using the six Monte Carlo simulation samples. Table 2 lists various efficiencies defined above calculated from the Monte Carlo, the error represent the statistic uncertainties. we have calculated the efficiencies for both ρ mass cut and K^* mass cut. Totally 12 efficiency factors are calculated.

Table 2. The Efficiencies Calculated from the Monte Carlo

Monte Carlo	$\epsilon_{\rho\ cut}$	$\epsilon_{K^*\ cut}$
$\psi\prime \rightarrow K_1^{\pm}(1270)K^{\mp} \rightarrow K^{\pm}\rho^0 K^{\mp}$	0.158 ± 0.013	0.050 ± 0.004
$J/\psi \rightarrow K_1^{\pm}(1270)K^{\mp} \rightarrow K^{\pm}\rho^0 K^{\mp}$	0.038 ± 0.006	0.019 ± 0.003
$\psi\prime \rightarrow K_1^{\pm}(1270)K^{\mp} \rightarrow K^{*0}\pi^{\mp}K^{\mp}$	0.053 ± 0.008	0.101 ± 0.017
$J/\psi \rightarrow K_1^{\pm}(1270)K^{\mp} \rightarrow K^{*0}\pi^{\mp}K^{\mp}$	0.017 ± 0.003	0.039 ± 0.006
$\psi\prime \rightarrow K_1^{\pm}(1400)K^{\mp} \rightarrow K^{*0}\pi^{\mp}K^{\mp}$	0.061 ± 0.005	0.136 ± 0.011
$J/\psi \rightarrow K_1^{\pm}(1400)K^{\mp} \rightarrow K^{*0}\pi^{\mp}K^{\mp}$	0.023 ± 0.004	0.044 ± 0.007

- Fitting and the branching ratios

  For the decay $K_1(1270) \rightarrow K\rho$, the peak near 1.27 GeV/c^2 in $K\rho$ mass distribution is not in Breit-Wigner form, because the resonance shape is distorted by the restricted phase space for this decay mode. A function $f_{K\rho}$ was proposed to take the distortion into account [1]. This function is the convolution of a s-wave $K_1(1270)$ Breit-Wigner function with a p-wave ρ meson Breit-Wigner function with their mass and width fixed at the PDG values. Here as a preliminary check, we fit the mass distribution with B-W peaks plus polynomial background. The results are shown in Fig.8. The event numbers from the fits and the calculated preliminary branching ratios are listed below (the errors are statistic):

Table 3. The event numbers and the branching ratios

decay	event number	branching ratio
$\psi\prime \rightarrow K1^{\pm}(1270)K^{\mp}$	87.9 ± 9.4	(9.0 ± 1.0)×10^{-4}
$\psi\prime \rightarrow K1^{\pm}(1400)K^{\mp}$	45.0 ± 6.7 (<53.6, 90% CL)	< 7.7 ×10^{-4}
$J/\psi \rightarrow K1^{\pm}(1270)K^{\mp}$	27.0 ± 5.2 (<33.7, 90% CL)	< 4.4 ×10^{-3}
$J/\psi \rightarrow K1^{\pm}(1270)K^{\mp}$	106.9 ± 10.3	(4.7 ± 0.5) ×10^{-3}

5 Conclusions

- Comparing the mass distributions and the preliminary branching ratios with the Hawaii group's results, we see that they are in agreement, although we use different strategy and different requirements in the event selection.

- Hawaii group's results shows the strong violations of the 15% rule and the SU3 symmetry for both channels. We see the same tendency, but the violation is not so prominent. This may be caused by the preliminary fitting method used in our analysis.

- By improving the accuracy in the fitting and the efficiency calculation, we'd expect a better agreement between the two analysis, because the mass distributions are similar.

Acknowledgments

We acknowledge the help of Prof. Yifan Gu, Dr. Xinhua Li and other members of the BES $\psi\prime$ group at IHEP. We also thank Prof. S. Olsen and Dr. D. Paluselli at the University of Hawaii, whose careful work on the same subject give us many inspirations in the analysis.

References

[1] S.L.Olsen, D.Paluselli, BES analysis memo.

[2] T.Applequist and D.Politzer, Phys. Rev. Lett. 34, (1975)43

[3] M.E.B. Franklin $et.al.$, Phys. Rev. Lett. 51, (1983)963.

[4] H.G.Blundell, S.Godfrey, and B.Phelps, Phys. Rev. D53, (1996)3712,
M. Suzuki, Pkys. Rev. D47, (1993)1252.

[5] R.M.Barnett $et.al.$, Particle Data Group), Phys. Rev. D54, (1996)1.

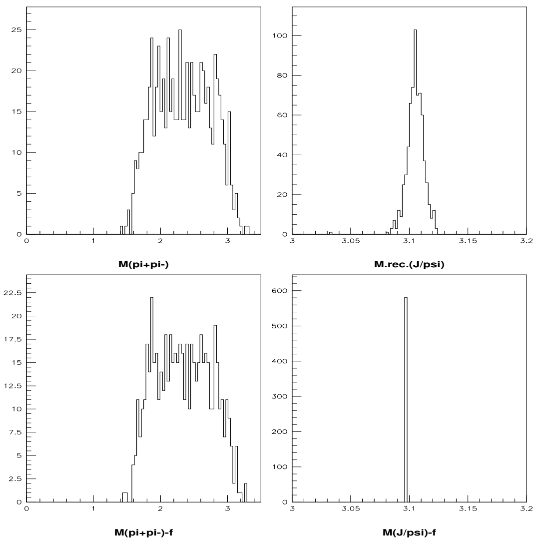

Figure 1: The recoil mass distributions of $\pi^+\pi^-$ for 6-prong data. Left side: the recoil mass distributions of the $\pi^+\pi^-$ pair not recoiling to J/ψ; right side: the recoil mass distributions of the $\pi^+\pi^-$ pair recoiling to J/ψ. Upper: recoil mass calculated using the information in 'trklst'; lower: recoil mass after telesis fit with a resonance at J/ψ.

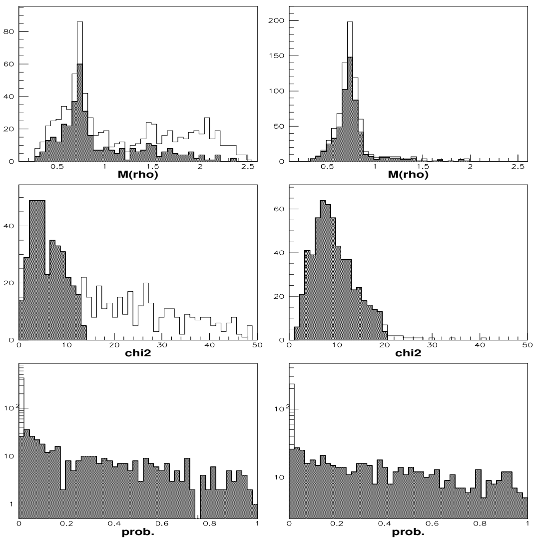

Figure 2: The effect of including $\sum \chi^2(dE/dx)$ in the kinamatic fit ($\psi\prime \to K_1^{\pm}(1270)$ Monte Carlo). Left side: using $\chi^2(4Cfit)$ only. Right side, using $\chi^2(4Cfit) + \sum \chi^2(dE/dx)$. Top: mass distributions of $\pi^+\pi^-$ (the shadowed area is the distribution after a cut at $Prob(\chi^2, n) > 0.01$, where $n = 4$ in the left side and $n = 8$ in the right side). Middle: the distribution of χ^2 (the shadowed area indicates the cut at $Prob(\chi^2, n) > 0.01$). Bottom the distribution of $Prob(\chi^2, n)$ (the shadowed area indicates the cut at $Prob(\chi^2, n) > 0.01$).

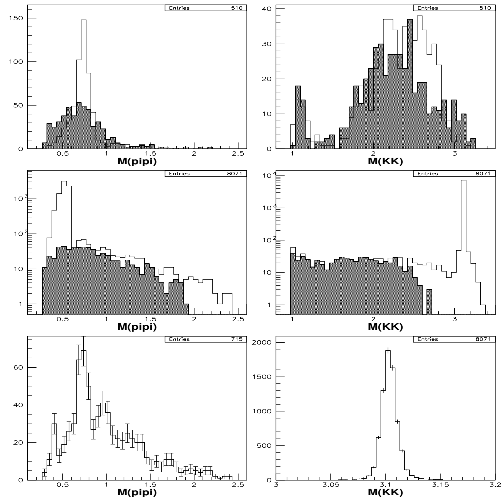

Figure 3: The invariant mass distributions of the $\pi^+\pi^-$ candidates (left side) and K^+K^- candidates (right side). Top: the histograms are for MC $\psi\prime \to K_1^{\pm}(1270)K^{\mp} \to K^{\pm}\rho^0(770)K^{\mp} \to K^+K^-\pi^+\pi^-$; the shadowed histograms are for MC $\psi\prime \to K_1^{\pm}(1400)K^{\mp} \to K^{*0}(892)\pi^{\pm}K^{\mp} \to K^+K^-\pi^+\pi^-$. Middle: the histograms are for 4-prong data, the shadowed histograms are for 6-prong data. Bottom: left plot is for 4-prong data after J/ψ cut, a clear $\rho(770)$ peak can be seen; right plot display the excluded J/ψ peak.

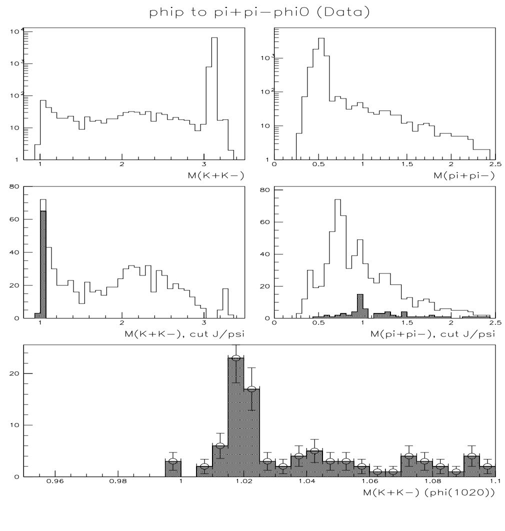

Figure 4: The invariant mass of K^+K^- and $\pi^+\pi^-$ showing the events come from $\psi\prime(J/\psi) \to \phi(1020)X$, and $\phi(1020) \to K^+K^-, X \to \pi^+\pi^-$ in the selected 4-prong data sample. Top: $M(K^+K^-)$ and $M(\pi^+\pi^-)$ before removing the $\psi\prime \to \pi^+\pi^-(J/\psi)$ contamination. Middle: after removing the $\psi\prime \to \pi^+\pi^-(J/\psi)$ events, the $\phi(1020)$ (the shadowed area in the left plot) and the recoiling $\pi^+\pi^-$ (the shadowed area in the right plot) are shown, a possible $f_0(980)$ is also seen in the mass distribution of $\pi^+\pi^-$ recoiling to the $\phi(1020)$. Bottom: the distribution of the $\phi(1020)$ peak in more detail.

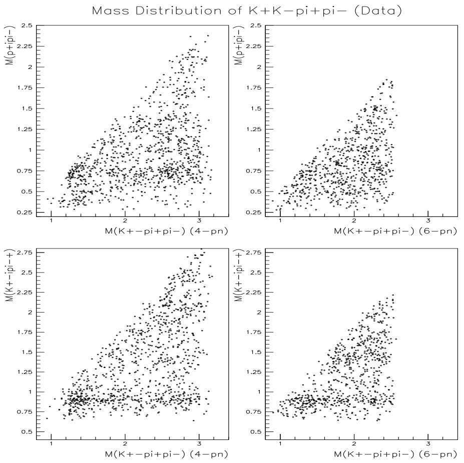

Figure 5: The invariant mass distributions of $\pi^+\pi^-$ .vs. $K^{\pm}\pi^+\pi^-$ (top) and $K^{\pm}\pi^{\mp}$ .vs. $K^{\pm}\pi^+\pi^-$ (bottom) are shown respectively for selected 4-prong events (left side) and 6-prong events (right side). Two possible particle combinations for each events ($K^+\pi^+\pi^-$ or $K^-\pi^+\pi^-$) are filled in the plots(2 entries/ per event). The band of $K^*(892)$ mass are seen quite clearly in $M(K^{\pm}\pi^{\mp})$ dimension for both 4-prong and 6-prong data, the $\rho(770)$ band are also seen for 4-prong data but not so obvious for 6-prong data. Some clustering of event near $K_1(1270)$ or $K_1(1400)$ mass are seen in $M(K^{\pm}\pi^+\pi^-)$ dimension for the 4-prong data, but not so obvious for the 6-prong data.

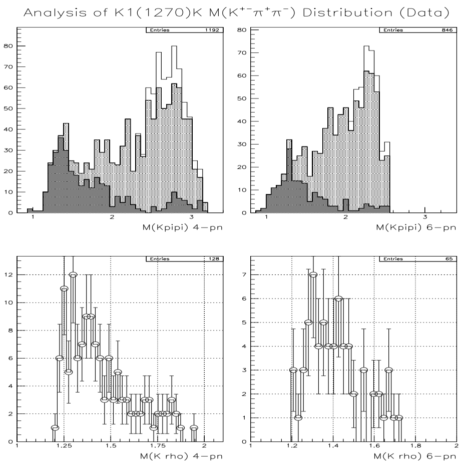

Figure 6: The invariant mass distributions of $K^{\pm}\pi^+\pi^-$ for 4-prong data (left) and for 6-prong data (right) respectively for $K_1(1270)$ analysis. The top plots show the effect of removing $\psi\prime(J/\psi) \to \phi X$ events (the shadowed area, still 2 entries / per event) and the effect of the helicity angle cut (the dark area, 1 entry / per event). We see most of the wrong combinations are removed by the $cos\theta > 0.75$ cut. The bottom plots shows the final $M(K^{\pm}\pi^+\pi^-)$ distributions after a cut at $\rho(770)$ mass (require $|M(\pi^+\pi^-) - 0.77| < 0.15$ GeV/c^2). The $K_1(1270)$ peak is seen in $M(K^{\pm}\pi^+\pi^-)$ for the 4-prong data ($\psi\prime \to K_1K$), while there seem to be also a heap around 1.4 GeV/c^2 for the 6-prong data ($J/\psi \to K_1K$).

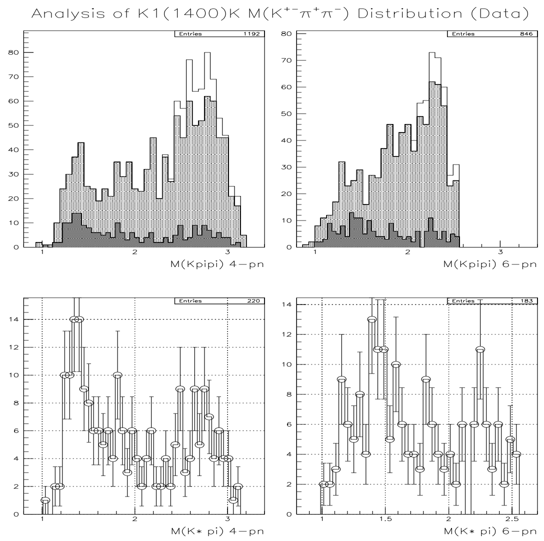

Figure 7: The invariant mass distributions of $K^{\pm}\pi^{+}\pi^{-}$ for 4-prong data (left) and for 6-prong data (right) respectively for $K_1(1400)$ analysis. The shadowed area in the top plots show the effect of removing $\psi\prime(J/\psi) \to \phi X$ events (2 entries / per event). Avoiding double counting by choosing one of $M(K^{\pm}\pi^{\mp}$ as described in the text and applying a $K^{*}(892)$ mass cut ($|M(K^{\pm}\pi^{\mp}) - M(K^{*}(892)| < 0.05$ GeV/c^2), the resulted $K^{\pm}\pi^{+}\pi^{-}$ distributions are shown in the bottom plots (also the dark area in the top plots). The $K_1(1400)$ peak is seen in the $M(K^{\pm}\pi^{+}\pi^{-})$ distributions for the 6-prong data ($J/\psi \to K_1 K$), while there seem to be a overlap of $K_1(1400)$ and $K_1(1270)$ in the distribution for the 4-prong data ($\psi\prime \to K_1 K$).

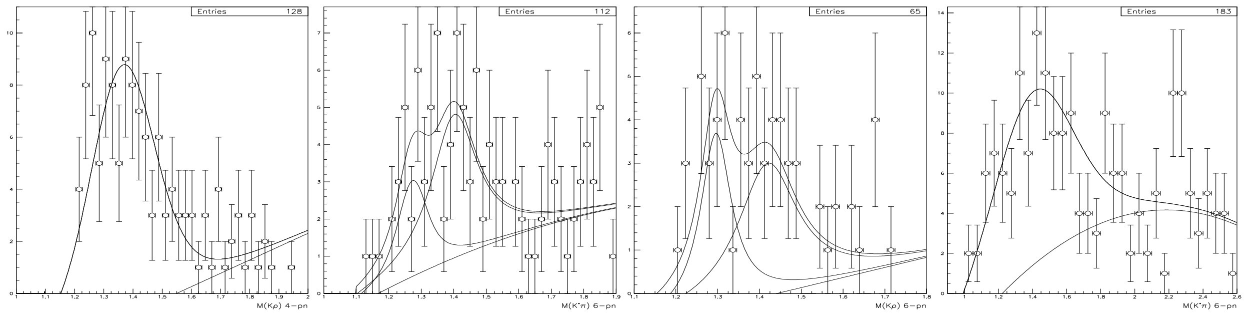

Figure 8: The preliminary Breig-Wigner + polynimial backgroung fitting for the four selected $K\pi^{+}\pi^{-}$ mass distributions after various cuts.